Quantum path-integral method for the fictitious-particle Hubbard model

Zhijie Fan [1,2,3,*] Tianning Xiao [1] and Youjin Deng [1,2,3,†]

[1] *Hefei National Research Center for Physical Sciences at the Microscale and School of Physical Sciences, University of Science and Technology of China, Hefei 230026, China*

[2] *Hefei National Laboratory, University of Science and Technology of China, Hefei 230088, China*

[3] *Shanghai Research Center for Quantum Science and CAS Center for Excellence in Quantum Information and Quantum Physics, University of Science and Technology of China, Shanghai 201315, China*

(Received 11 August 2025; revised 30 January 2026; accepted 3 February 2026; published 11 March 2026)

We formulate a path-integral Monte Carlo algorithm for simulating lattice systems consisting of fictitious particles governed by generalized exchange statistics. This method, initially proposed for continuum systems, introduces a continuous parameter ξ in the partition function that interpolates between bosonic ($\xi = 1$) and fermionic ($\xi = -1$) statistics. We generalize this approach to discrete lattice models and apply it to the two-dimensional Hubbard model of fictitious particles, including the Bose- and Fermi-Hubbard models as special cases. By combining reweighting and ξ-extrapolation techniques, we access both half-filled and doped regimes. In particular, we demonstrate that the method remains effective in strongly correlated, doped systems, offering a distinct advantage by naturally operating in the canonical ensemble. Our results validate the applicability of the fictitious-particle framework to lattice models and establish it as a promising, complementary tool for investigating strongly interacting fermionic systems.

DOI: 10.1103/vqj6-6vyt

I. INTRODUCTION

The Quantum Monte Carlo (QMC) method is one of the most powerful and versatile numerical techniques for investigating quantum many-body systems, with broad applications across diverse areas of physics [1–3]. By reformulating the partition function as a weighted sum over configurations in a chosen computational basis, QMC employs importance sampling to efficiently explore the exponentially large configuration space. However, when applied to fermionic systems, QMC suffers from the notorious "fermion sign problem" [4]: configuration weights oscillate in sign due to the antisymmetric nature of fermionic wave functions, leading to severe cancellations and overwhelming statistical noise. As a result, the computational cost required to achieve a given accuracy grows exponentially with both the system size and the inverse temperature, severely limiting the applicability of QMC to many important fermionic systems [5].

A prominent example is the Fermi-Hubbard model [6], a paradigmatic strongly correlated lattice fermion system that is closely related to the mechanism of high-temperature superconductivity and the origin of quantum magnetism [7,8]. Over the past 60 years, remarkable progress has been made in numerical [9,10] and experimental [11,12] studies of this model. Yet, obtaining unbiased solutions of the Hubbard model at generic fillings and interaction strengths remains an outstanding challenge. The determinant quantum Monte Carlo (DQMC) method has been widely used for exploring the equilibrium properties of interacting fermions [13–16]. It is formulated in the grand-canonical ensemble and, more importantly, is sign-problem-free at half-filling on bipartite lattices due to particle-hole symmetry, making it a highly efficient tool to investigate the Fermi-Hubbard model in various parameter regimes. However, away from this special point, the sign problem reemerges and worsens rapidly, posing challenges to the computational efficiency of DQMC [15].

The fermion sign problem has been proven to be nondeterministic polynomial-time hard [5], implying that finding a generic solution to it is extremely difficult, if not impossible. Despite this inherent difficulty, significant progress has been made in developing approaches that alleviate or avoid the sign problem in specific models or parameter regimes [17,18], including the diagrammatic QMC [19], the Lefschetz thimble method [20,21], the Majorana representation QMC [22], the constrained-path QMC [23], and the sign bound theory [24]. These developments underscore the need for new conceptual frameworks to broaden the applicability of QMC to fermionic systems.

Very recently, a novel approach to circumvent the fermion sign problem based on the Path Integral Molecular Dynamics (PIMD) simulations of fictitious particles was proposed by Xiong and Xiong [25–27]. In this framework, the canonical partition function is parametrized by a continuous parameter $\xi \in \mathbb{R}$, which defines a family of fictitious identical particles with generalized exchange statistics interpolating between Bose-Einstein ($\xi = 1$) and Fermi-Dirac ($\xi = -1$) limits. By carrying out PIMD simulations of fictitious particles in the $\xi > 0$ sector, where all configuration weights remain strictly positive, thus avoiding the fermion sign problem, one can then

*Contact author: zfanac@ustc.edu.cn

†Contact author: yjdeng@ustc.edu.cn

extrapolate the physical observables to the fermionic limit of $\xi = -1$ [25–27].

The fictitious-particle framework has achieved notable success in simulating interacting fermion systems in continuous space. Early PIMD studies introduced and applied the ξ-extrapolation method to the interacting fermion gas, showing that the energy of the system can be accurately obtained using an empirical quadratic fit in ξ [25]. Subsequent work by Dornheim *et al*. using Path Integral Monte Carlo (PIMC) demonstrated that the ξ-extrapolation method yields excellent agreement with benchmark results for various observables in weakly degenerate systems, such as structure factors and radial distribution functions [28]. In particular, for the warm dense uniform electron gas, they report a speedup exceeding 11 orders of magnitude over direct fermion PIMC simulations. In a recent study, Dornheim *et al*. [29] employed the fictitious-particle PIMC to perform highly accurate simulations of the warm dense electron gas, achieving system sizes of up to ∼1000 particles. Furthermore, the fictitious-particle PIMC method has recently enabled the first *ab initio* interpretation of x-ray Thomson scattering (XRTS) measurements on strongly compressed beryllium [30]. Although the ξ-extrapolation becomes ineffective at low temperatures, a refined extrapolation strategy guided by the physical properties of the fictitious particles has been developed to study the thermodynamic properties of fermions at arbitrary temperatures [31]. The method has been successfully employed to study the normal liquid state of Helium-3, a system with high quantum degeneracy, providing energy values that match experimental measurements [32]. Despite these successes, the application of the fictitious-particle framework has thus far been restricted to continuous-space models. Extending this approach to lattice systems represents a compelling direction for future research, offering the possibility of alleviating the fermion sign problem in a broader class of models and accessing parameter regimes that remain challenging for conventional QMC methods.

In this work, we extend the fictitious-particle framework to discrete lattice models and develop a PIMC algorithm for fictitious identical particles on a lattice. Specifically, we apply the algorithm to the two-dimensional (2D) Hubbard model of fictitious particles in the canonical ensemble and evaluate its effectiveness for investigating the corresponding fermionic model. We implement a ξ-based reweighting scheme and assess its applicability to both half-filled and doped cases, showing that this seemingly simple approach remains effective in the strong-coupling regime. Furthermore, we show that ξ-extrapolation further broadens the applicability of reweighting. Together, these techniques establish the fictitious-particle framework as a complementary tool for investigating strongly interacting fermionic systems, particularly offering distinct advantages in the canonical ensemble and at extreme interaction strengths where conventional methods face challenges.

The paper is organized as follows: Section II gives a brief introduction to fictitious-particle formalism. In Sec. III, we formulate the path-integral representation of fictitious particles on a lattice and present the corresponding PIMC algorithm. Section IV applies the fictitious-particle PIMC method to the two-dimensional Hubbard model to evaluate the performance of the method. Section V demonstrates the application of the ξ-extrapolation technique. Finally, in Sec. VI, we discuss the broader applicability, limitations, and future directions of the method.

II. PARTITION FUNCTION OF FICTITIOUS IDENTICAL PARTICLES

The quantum statistical partition function for a system characterized by Hamiltonian $\mathcal{H}$ is defined as

$$\mathcal{Z} = \mathrm{Tr}[e^{-\beta\mathcal{H}}] \tag{1}$$

$$= \sum_{\alpha} \langle\Psi_\alpha|e^{-\beta\mathcal{H}}|\Psi_\alpha\rangle, \tag{2}$$

where $\beta \equiv 1/T$ is the inverse temperature, and $\{|\Psi_\alpha\rangle\}$ represents an orthonormal and complete basis in the Hilbert space of $\mathcal{H}$. For a system of N distinguishable particles, each having M possible single-particle states, the Hilbert space dimension is M^N. A basis vector can be represented as

$$|\Psi_\alpha\rangle = |\psi_1, \psi_2, \ldots, \psi_N\rangle, \tag{3}$$

where ψ_i labels the state of the ith particle in a chosen single-particle basis, e.g., spatial position, spin. An arbitrary wave function in this space is a linear combination of basis vectors $|\Phi\rangle = \sum_\alpha c_\alpha|\Psi_\alpha\rangle$ with normalized coefficients satisfying $\sum_\alpha |c_\alpha|^2 = 1$. For identical particles, the many-body wave function must be symmetric under particle exchange for bosons and antisymmetric for fermions. The physical Hilbert space is constructed from basis states that satisfy the required exchange symmetry. A convenient choice for both bosons and fermions is the occupation number representation, where the allowed occupations are $n_i = 0, 1, 2, \ldots$ for bosons and $n_i = 0, 1$ for fermions.

An alternative way to express the canonical partition function of N identical particles is to incorporate the effects of particle exchanges explicitly,

$$\mathcal{Z}_\pm(T) = \frac{1}{N!}\sum_{P\in S_N}\sum_{\alpha}(\pm 1)^{N_P}\langle\Psi_\alpha|e^{-\beta\mathcal{H}}|P(\Psi_\alpha)\rangle, \tag{4}$$

where the factor -1 corresponds to fermions and $+1$ to bosons [25,26]. The first summation goes over all permutations in the S_N permutation group, which consists of $N!$ elements. Here, N_P is the exchange number of P, defined as the minimal number of pairwise swaps to recover the original order from permutation P. A permutation P acts on a basis $|\Psi\rangle$ by reassigning particle labels, such that the state of the ith particle is mapped to the $P(i)$th particle, resulting in a permuted basis state

$$|P(\Psi)\rangle = |\psi_{P(1)}, \psi_{P(2)}, \ldots, \psi_{P(N)}\rangle. \tag{5}$$

For fermions, the summation in the partition function can have negative terms when N_P is odd. This could eventually invalidate the probabilistic interpretation of configuration weights in QMC sampling, leading to the fermion sign problem [17,33].

To alleviate the sign problem, Ref. [25] proposes a generalized partition function,

$$\mathcal{Z}_\xi(T) = \frac{1}{N!}\sum_{P\in S_N}\sum_{\alpha}\xi^{N_P}\langle\Psi_\alpha|e^{-\beta\mathcal{H}}|P(\Psi_\alpha)\rangle, \tag{6}$$

where ξ is a real number, allowing one to continuously interpolate between fermionic ($\xi = -1$) and bosonic ($\xi = 1$) statistics. In the bosonic sector $\xi > 0$, the negative sign due to particle exchanges is absent. When $|\xi| < 1$, the contribution from particle permutations is suppressed; at $\xi = 0$, all exchange terms vanish, corresponding to an idealized model of distinguishable quantum particles known as Boltzmannons [28]. The fictitious-particle formulation thus provides a framework that smoothly connects bosonic, fermionic, and distinguishable particle limits, and forms the basis for developing a path-integral Monte Carlo algorithm that operates in the $\xi > 0$ regime to circumvent the fermion sign problem.

III. PATH-INTEGRAL METHOD FOR FICTITIOUS PARTICLES ON LATTICE

In this section, we formulate the path-integral representation for fictitious particles on lattices, building upon the generalized partition function defined in Eq. (6). We develop a PIMC algorithm that employs a modified worm update scheme by explicitly incorporating the particle exchange number N_P, thereby enabling direct simulation of fictitious particles in the $\xi > 0$ sector. Furthermore, we implement a reweighting scheme in ξ to estimate physical observables in the $\xi < 0$ regime based on simulations performed at $\xi > 0$. Together, the modified worm algorithm and the ξ-reweighting scheme provide a framework for studying lattice models with generalized quantum statistics.

A. Path-integral formalism for fictitious particles

The central idea of the PIMC method [16,34–36] is to map a d-dimensional quantum system onto an equivalent $(d+1)$-dimensional classical system by expanding the quantum partition function in a suitable basis. In this mapping, the additional dimension corresponds to the imaginary time (τ) axis with periodic boundary conditions (PBCs). The quantum statistical properties are then extracted by sampling configurations in the classical system. Each configuration consists of a sequence of states along the imaginary-time axis, forming continuous trajectories in the $(d+1)$-dimensional space, namely the worldlines. For a system with particle number conservation, the trajectories of particles are closed loops. The partition function of the original quantum model is then represented as a weighted sum over all possible worldline configurations in $(d+1)$-dimensional space time.

We consider a generic lattice system of N particles governed by the Hamiltonian $\mathcal{H} = \hat{K} + \hat{V}$. Here, we adopt a specific many-body basis $\{|\alpha\rangle\}$, referred to as the configuration basis (e.g., real-space position basis). The Hamiltonian is decomposed such that $\hat{V}$ represents the diagonal part, satisfying $\hat{V}|\alpha\rangle = V_\alpha|\alpha\rangle$, where V_α corresponds to the potential energy of the configuration $|\alpha\rangle$. The term $\hat{K}$ contains the off-diagonal terms that generate transitions between basis states.

A crucial distinction in our fictitious-particle framework, compared to conventional lattice PIMC methods, lies in the treatment of particle indistinguishability. Conventional methods typically employ the occupation number basis $|n_1, n_2, \ldots\rangle$, where particle exchange is treated implicitly. In contrast, we employ a basis where particles are explicitly labeled and thus distinguishable. For instance, in a system with two particles on distinct sites i and j, the states $|i, j\rangle$ and $|j, i\rangle$ are treated as orthogonal and distinct configurations.

The derivation of the path-integral representation does not depend on the specific choice of basis. Starting from the generalized partition function in Eq. (6), we apply the Trotter-Suzuki decomposition with M time slices of width $\epsilon = \beta/M$. To account for quantum statistics in this distinguishable basis, we must sum over all particle permutations P connecting the initial and final states:

$$\mathcal{Z}_\xi = \lim_{M\to\infty} \frac{1}{N!} \sum_{P\in S_N} \xi^{N_P} \sum_{\alpha_0} \langle \alpha_0 | (e^{-\epsilon \hat{K}} e^{-\epsilon \hat{V}})^M | P(\alpha_0)\rangle. \quad (7)$$

Here, $|P(\alpha_0)\rangle$ represents the basis state where particle labels are permuted according to P. By inserting complete sets of basis states $\{|\alpha_k\rangle\}$ at each time slice, the trace becomes a sum over discrete paths satisfying the boundary condition $|\alpha_M\rangle = |P(\alpha_0)\rangle$.

In the continuous-time limit ($M \to \infty, \epsilon \to 0$), we obtain an exact path-integral representation. The total configuration space decomposes into distinct topological sectors, each labeled by a specific permutation P. The extended partition function is the sum over these sectors:

$$\mathcal{Z}_\xi = \frac{1}{N!} \sum_{P\in S_N} \xi^{N_P} \int \mathcal{D}\mathcal{C}_P \, w(\mathcal{C}_P). \quad (8)$$

Here, $\int \mathcal{D}\mathcal{C}_P$ denotes the integration over all continuous worldline configurations $\mathcal{C}_P$ that satisfy the specific boundary condition imposed by P. The weight of such a configuration is

$$w(\mathcal{C}_P) = \left(\prod_{k=1}^{n} \langle \alpha_k | (-\hat{K}) | \alpha_{k-1} \rangle \right) \exp\left[-\int_0^\beta V_{\alpha(\tau)} d\tau \right]. \quad (9)$$

Crucially, while the partition function formally sums over all permutations, for any single closed worldline configuration generated in the path integral, the permutation P is uniquely determined. In the $(d+1)$-dimensional space-time, particle trajectories form closed loops. The specific permutation P associated with a configuration can be explicitly identified by tracing the continuous path of each particle label from $\tau = 0$ to $\tau = \beta$. If the trajectory starting at position r_i (label i) connects to the position r_j (label j) at $\tau = \beta$, it signifies a permutation involving these indices. The exchange number N_P is thus a direct topological property of the worldline configuration.

Although the fictitious-particle PIMC framework does not prohibit multiple occupancy, its direct implementation on a lattice benefits significantly from adopting a hardcore-particle basis. First, unlike in continuous-space PIMC, where the probability of two particles occupying the exact same coordinate is negligible, worldlines in lattice models frequently visit the same site simultaneously. This makes tracking individual particle trajectories technically cumbersome, as shown in Fig. 1(a). By simulating hardcore particles, worldlines of the same particle species never occupy the same site, rendering the total permutation well-defined and straightforward to track [see Fig. 1(b)]. Second, the hardcore basis is naturally suited for studying the fermion limit $\xi \to -1$, where the Pauli exclusion principle strictly prohibits two identical fermions

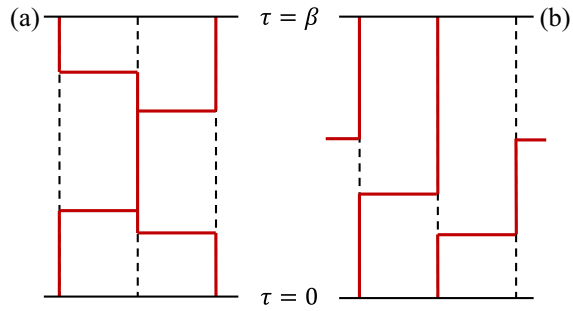

FIG. 1. Schematic diagram of worldline configuration of a lattice model for (a) softcore particles and (b) hardcore particles. In panel (a), the solid line represents the path of softcore particles along the imaginary time direction, whose trajectories can intersect. (b) shows a worldline configuration of hardcore particles where the paths of different particles cannot intersect. The worldlines of two particles connect at $\tau = \beta$, corresponding to a particle permutation, with $N_P = 1$ in this case.

from occupying the same state. At $\xi = -1$, contributions from configurations with intersecting worldlines would cancel out. Therefore, the hardcore particle basis naturally aligns with fermionic statistics in the $\xi \to -1$ limit, eliminating redundant sampling of canceling configurations and thereby enhancing algorithmic efficiency.

Under the hardcore-particle constraint, the total number of particle exchanges, N_P, is uniquely determined for each worldline configuration. This quantity arises naturally from the cycle decomposition of the underlying permutation P. In the worldline configuration, each distinct closed loop that winds along the imaginary time direction then corresponds to one cycle of P, and its winding number l equals the cycle length. Mathematically, a cycle of length l can be decomposed into $l - 1$ pairwise transpositions. Therefore, the total exchange number of the worldline configuration is

$$N_P = \sum_{\text{cycles}} (l - 1) = N - N_c, \tag{10}$$

where N is the total number of particles and N_c is the number of closed loops in the worldline configuration.

B. Worm update scheme for fictitious particles

The worldline configuration of hardcore particles can be efficiently sampled using the worm algorithm, which has been highly successful in simulating various quantum and classical systems [35–39]. The worm algorithm operates in an enlarged configuration space by introducing an open-ended worldline known as a "worm." The worm's "head" and "tail" correspond to annihilation (b) and creation ($b^\dagger$) operators, respectively. Conventionally, the b point is called *Ira*, and the $b^\dagger$ point is called *Masha*. The worldline configurations, consisting of closed particle trajectories, then form the Z configuration space, while configurations that consist of worms form the G space. Through local updates of *Ira* and *Masha* in the G space, the algorithm efficiently samples the configuration with different winding numbers, and particle permutations (reconnecting two paths). The measurements are then performed when the configuration is back in Z space. Despite being a local update scheme, the worm algorithm generally has a much smaller dynamical critical exponent than the Metropolis-type updates [35,37]; thus, it can be very efficient even near a phase transition.

A minimal worm algorithm of hardcore particles on a lattice system consists of the following updates:

(1) Create/delete the worm: A worm is created on a randomly chosen segment (a graphical element along the imaginary axis where the state on a lattice site remains unchanged) or deleted when there is no obstacle between Ira and Masha.

(2) Move the worm head: Masha is moved along the imaginary time.

(3) Insert/delete a kink after a worm head: a kink is inserted or deleted at an imaginary time after the Masha, and the position of the Masha is changed.

(4) Insert/delete a kink before a worm head: a kink is inserted or deleted at an imaginary time before the Masha, and the position of the Masha is changed.

This set of update operations ensures ergodicity, allows changing the configuration's winding number, and performs particle exchange.

In this work, we focus on the canonical ensemble, in which the total number of particles is fixed. The conventional method of imposing the canonical ensemble in the worm algorithm is to restrict the temporal distance between the two worm heads (Ira and Masha) during the updates:

$$|\tau_{\text{Ira}} - \tau_{\text{Masha}}| < \beta/2. \tag{11}$$

In a particle-conserving system, worldlines form closed trajectories that wind across the periodic boundary in the imaginary-time axis. Consequently, the total particle number is topologically equivalent to the total worldline winding number along the imaginary-time axis. The constraint in Eq. (11) geometrically prevents the worm from completing such a winding or unwinding process along the temporal direction, thereby ensuring that the total particle number remains unchanged. This constraint is enforced in all updates that modify the worm head in the temporal direction, including the create, delete, and move worm updates. Moreover, the hardcore limit is imposed by rejecting any proposed update that generates segments with occupation larger than 1.

The key difference between our approach and the conventional worm algorithm [35] lies in the configuration weight. In the fictitious-particle framework, the configuration weight is proportional to ξ^{N_P}. Therefore, unlike the standard algorithm, in which topological sectors typically do not affect the weight of intermediate worm configurations, our method requires tracking of the exchange number N_P during worm updates. This dependency means that the instantaneous value of N_P directly affects the acceptance probability of the updates. To incorporate the generalized exchange statistics, we continuously track N_P within the G space using the generalized relation $N_P = N - N_c$, where N_c is the number of worldline clusters. A worldline cluster is defined as a connected set of worldline segments and kinks; thus, both closed loops and the worm (open trajectory) count as clusters. This definition ensures that the exchange number remains consistent with its physical definition when the worm is eventually removed.

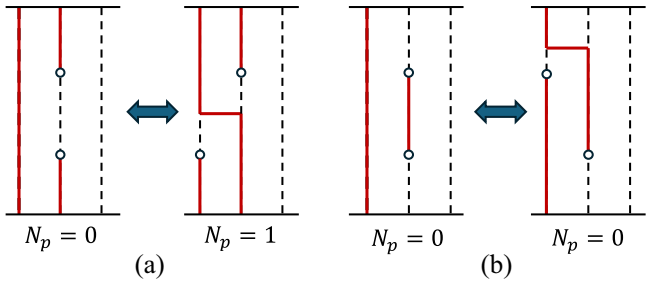

FIG. 2. Insert/delete kink updates that (a) change N_P and (b) do not change N_P. In panel (a), a worm is created by opening an existing worldline, resulting in two disconnected clusters. Inserting a kink that connects two different worldlines reduces the number of clusters N_c by 1 and increases the total exchange number N_P by 1. In (b), a worm is created by inserting a new worldline with length smaller than $\beta/2$, which is not associated with any physical particle. After kink insertion, N_P remains unchanged, as this worm does not contribute to the physical permutation.

Using this general definition, we can explicitly update and sample N_P along with worm moves. In our PIMC algorithm for fictitious particles, only kink-insertion and kink-deletion moves can alter the total exchange number N_P, since they change the connectivity of worldline clusters — analogous to the swap update in continuous-space PIMC [32]. Specifically, the *insert kink after worm head* update proposes a new creation-annihilation operator pair after the worm head (Masha), moving the worm head from its current site to a neighboring site. If the update connects Masha to a worldline cluster distinct from its current one, two disjoint clusters merge, reducing the number of disjoint cycles N_c by 1; thus, $N_P = N - N_c$ increases by 1, see Fig. 2(a). Conversely, if Masha connects to a segment within its own cluster, a closed loop is detached and N_P decreases by 1.

A technical special consideration is necessary in the above definition of N_P in G space for the "short worms" cases—open trajectories with a temporal span less than $\beta/2$, originating from creating a worm on an empty segment. In standard worm implementations, such details are often irrelevant. However, these short, isolated worms are transient auxiliary structures in our framework that need special consideration. Due to the canonical constraint in Eq. (11), the update of a short worm alone will not change the permutation of configurations. Only after it has been merged to another worldline that is longer than $\beta/2$, the worm updates can then change the connectivity of worldlines. Therefore, we need two specific handling rules for these cases. First, N_c counts only those clusters whose length in the imaginary time direction exceeds $\beta/2$. Second, when a short worm is connected to another worldline, the total N_c remains unchanged, as shown in Fig. 2(b). This ensures the detailed balance condition for updates involving short worms. We note that this handling of short worms is an implementation-specific detail; for instance, it would not arise if one restricted worm creation solely to opening existing worldlines. However, addressing it explicitly ensures the robustness of the algorithm.

Finally, we emphasize that the proposal scheme for all updates remains identical to the standard worm algorithm [35]. The generalized exchange statistics only affect the acceptance probability of the kink-insertion and deletion moves, which are responsible for changing N_P. The acceptance probability for a kink insertion or deletion then includes both energetic contributions and an additional statistical factor arising from particle exchange:

$$p_{\text{accept}} = \min\left[1, \frac{p(\mathcal{C} \to \mathcal{C}')w(\mathcal{C}')}{p(\mathcal{C}' \to \mathcal{C})w(\mathcal{C})}\xi^{\Delta N_P}\right], \tag{12}$$

where ΔN_P is the change in the particle exchange number due to the proposed update, and $p(\mathcal{C} \to \mathcal{C}')$ is the proposal probability of the update.

C. Reweighting measurement technique

The generalized partition function in Eq. (6) not only allows direct simulations of fictitious particles for $\xi > 0$, but also enables a direct reweighting to $\xi < 0$. The reweighting technique is a powerful numerical method used in Monte Carlo simulations to efficiently obtain physical observables across different parameter regimes without performing extensive independent simulations. One typically simulates the system at a given parameter and reweights the distribution to estimate the physical observables at different parameters near the original one.

The partition function of fictitious particles has the form

$$\mathcal{Z} \propto \sum_{\{\mathcal{C}\}} \xi^{N_P} w(\mathcal{C}). \tag{13}$$

One can then apply the reweighting method to ξ. Specifically, during a simulation performed at a certain ξ_0, we measure observables at another target ξ by reweighting the measurement with the factor $(\xi/\xi_0)^{N_P}$. The expectation value of an observable O at ξ is then given by

$$\langle O\rangle_\xi = \frac{\langle O \times (\xi/\xi_0)^{N_P}\rangle_{\xi_0}}{\langle(\xi/\xi_0)^{N_P}\rangle_{\xi_0}}, \tag{14}$$

where $\langle\cdot\rangle_{\xi_0}$ is the ensemble average at ξ_0. Note that the reweighting should not be performed at $\xi_0 = 0$, where all configurations with $N_P \neq 0$ are forbidden.

In principle, the reweighting method allows us to evaluate physical observables at arbitrary values of ξ using data obtained from a simulation performed at a fixed reference point $\xi_0 \neq 0$. However, one should not reweight to a target parameter that is too far from ξ_0. For each reweighting target ξ starting from a simulation at ξ_0, we measure the expectation value of $(\xi/\xi_0)^{N_P}$, which corresponds to the ratio of the partition functions at the two parameters:

$$\langle(\xi/\xi_0)^{N_P}\rangle = \frac{Z_\xi}{Z_{\xi_0}}. \tag{15}$$

This quantity measures the average reweighting factor when transitioning from a simulation performed at ξ_0 to a target parameter ξ, thereby directly characterizing the statistical efficiency of the reweighting scheme. When the target $\xi < 0$, we can interpret this ratio as a generalized sign, denoted as $s(\xi_0 \to \xi)$, which measures the magnitude of the sign problem of fictitious-particle PIMC simulation. In particular, the conventional fermionic sign corresponds to $s(1 \to -1)$.

This reweighting framework provides an approach for probing quantum statistics and fermionic limits. When the generalized sign remains of order $\mathcal{O}(1)$, the sign problem is mild, and reweighting can be performed efficiently with well-controlled statistical errors. In practice, the reweighting approach is found to be rather effective in the intermediate-temperature regime or under strong interactions, where it enables direct estimation of observables in the fermionic limit.

IV. HUBBARD MODEL OF FICTITIOUS PARTICLES

In this work, we apply the fictitious-particle PIMC method to the fictitious-particle Hubbard model on a square lattice, a generalized Hubbard model of hardcore fictitious particles that interpolates between the two-component hardcore Bose-Hubbard model and the Fermi-Hubbard model. By studying this model, we can probe the properties of the Fermi-Hubbard model, which suffers from a severe sign problem in certain important parameter regimes. The Hamiltonian of the fictitious-particle Hubbard model is given by

$$\mathcal{H}_\xi = -t\sum_{\langle i,j\rangle}(a^\dagger_{i\sigma}a_{j\sigma} + \text{H.c.}) + U\sum_i n_{i\uparrow}n_{i\downarrow}, \tag{16}$$

where t is the nearest-neighbor hopping strength and $U > 0$ is the on-site repulsive interaction. Throughout this work, we set $t = 1$ to define the unit of energy. The operator $a^\dagger_{i\sigma}$ ($a_{i\sigma}$) is the creation (annihilation) operator of a fictitious particle on the ith site with (pseudo-)spin $\sigma = \uparrow, \downarrow$, and $n_{i\sigma} = a^\dagger_{i\sigma}a_{i\sigma}$ is the corresponding number operator. The sum in the hopping term is over all nearest neighbors. The model reduces to the Fermi-Hubbard model when $\xi = -1$, and to a two-component hardcore Bose-Hubbard model when $\xi = 1$, which itself exhibits a variety of interesting phenomena [40,41].

In this case, because the single-particle spin is a good quantum number, we treat each spin component as a separate species and sample permutations independently within each component [32]. The worldline configuration thus has two components, one for each spin type. The worldlines in different components do not intersect or connect to each other. The total permutation of a configuration can be factorized as $P = P_\uparrow P_\downarrow$, where $P_\uparrow$ is a permutation among particles with up spin, and $P_\downarrow$ is a permutation among particles with down spin. Thus, the total exchange number is $N_P = N_{P_\uparrow} + N_{P_\downarrow}$. We perform QMC simulation in the $\xi > 0$ regime using the algorithm formulated in the previous section. During the update, the worm is created on a random component and updates only that spin component until the worm is deleted.

To characterize the system, we measure the following quantities for a given worldline configuration:

(1) The total energy

$$E = \frac{n_k}{\beta} + \frac{U}{\beta}\sum_i\int_0^\beta d\tau n_{i\uparrow}(\tau)n_{i\downarrow}(\tau), \tag{17}$$

where n_k is the total number of kinks in the worldline configuration. The first term represents the kinetic contribution, and the second term represents the on-site interaction energy.

(2) The fraction of lattice sites occupied by two particles,

$$d = \frac{1}{L^2}\sum_i\int_0^\beta d\tau n_{i\uparrow}(\tau)n_{i\downarrow}(\tau). \tag{18}$$

Here, L is the linear size of the system.

(3) The staggered magnetization M_{stagger}, which quantifies antiferromagnetic (AFM) spin correlations across the lattice, is defined as

$$M_{\text{stagger}} = \frac{1}{L^2}\int_0^\beta d\tau\sum_i(-1)^{x_i+y_i}S^z_i(\tau), \tag{19}$$

where $S^z_i = \frac{1}{2}(n_{i\uparrow} - n_{i\downarrow})$ is the spin component in the z direction on the ith site and x_i, y_i are the coordinates of the ith site.

During the simulation, we measure the following physical observables,

(1) Energy density $\varepsilon = \langle E\rangle/L^2$.

(2) Double occupancy $\langle n_{i\uparrow}n_{i\downarrow}\rangle \equiv \langle d\rangle$.

(3) AFM structure factor $S(\pi,\pi) = L^2\langle M^2_{\text{stagger}}\rangle$.

The $\langle\cdot\rangle$ represents the Monte Carlo average. The statistical error of simple observables is obtained by the binning method. For reweighted observables, the error is estimated using the Jackknife method.

To study the fermionic regime, we reweight the measured observables to various values of $\xi < 0$. To monitor the sign problem and the efficiency of reweighting, we also measure the generalized sign,

$$s(\xi_0 \to \xi) = \langle(\xi/\xi_0)^{N_P}\rangle. \tag{20}$$

This quantity characterizes the average statistical weight of configurations under reweighting from a reference value ξ_0 to a target ξ.

A. Benchmark with exact diagonalization

As a benchmark, we compare the results of fictitious-particle PIMC and the exact diagonalization (ED) method on a small system.

To perform exact diagonalization for lattice models of fictitious particles, we begin by explicitly constructing the many-body Hilbert space in the real-space basis $|x_1, x_2, \ldots x_N\rangle$. Each basis state represents a valid configuration of distinguishable quantum particles on the lattice, respecting the hardcore constraint. The total size of the Hilbert space of N hardcore particles on M sites is $M!/(M-N)!$, which is much larger than the conventional occupation basis for indistinguishable quantum particles. For particles with spin degrees of freedom, basis states are represented as ordered lists of occupied sites for each spin component $|x_{\uparrow,1}, x_{\uparrow,2}, \ldots x_{\uparrow,N_\uparrow}; x_{\downarrow,1}, x_{\downarrow,2}, \ldots x_{\downarrow,N_\downarrow}\rangle$.

The generalized quantum statistics of particles is recovered by explicitly incorporating the full permutation group S_N. We first diagonalize the Hamiltonian matrix in the distinguishable particle basis. Then, for each eigenstate of the Hamiltonian $|\phi_j\rangle$, we compute its overlap with all permuted copies of itself, $\langle\phi_j|P(\phi_j)\rangle$, and evaluate the generalized partition function:

$$\mathcal{Z}_\xi(T) = \frac{1}{N!}\sum_j e^{-\beta E_j}\sum_{P\in S_N}\xi^{N_P}\langle\phi_j|P(\phi_j)\rangle. \tag{21}$$

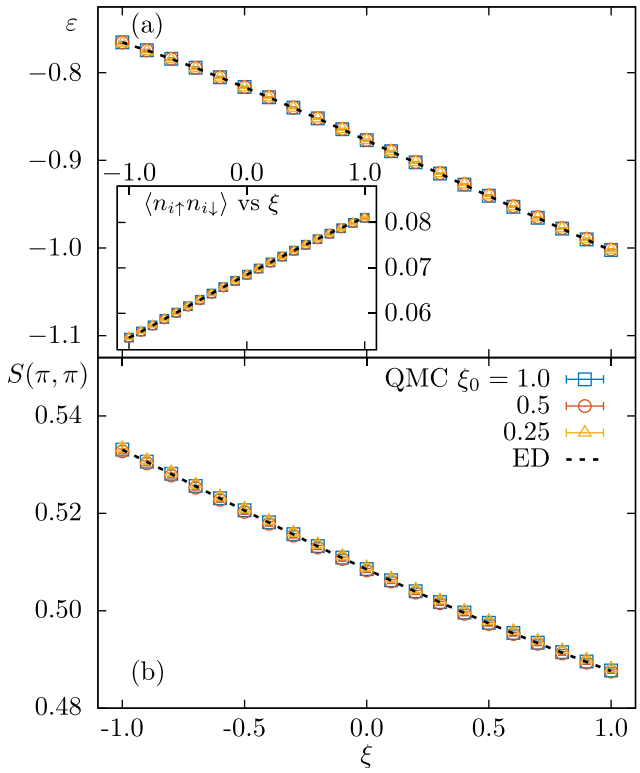

FIG. 3. Comparison between QMC and ED results for a half-filled fictitious-particle Hubbard model on a 2×2 square lattice with PBCs. The model parameters are $U = 10$ and $\beta = 1$. Note that the results are obtained in the canonical ensemble with fixed particle numbers $N_\uparrow = 2$ and $N_\downarrow = 2$. Panels show various observables as a function of ξ: (a) energy density ε, (inset) double occupancy $\langle n_{i\uparrow}n_{i\downarrow}\rangle$, and (b) AFM structure factor $S(\pi, \pi)$. The QMC results are obtained via reweighting from simulations at different ξ_0 values.

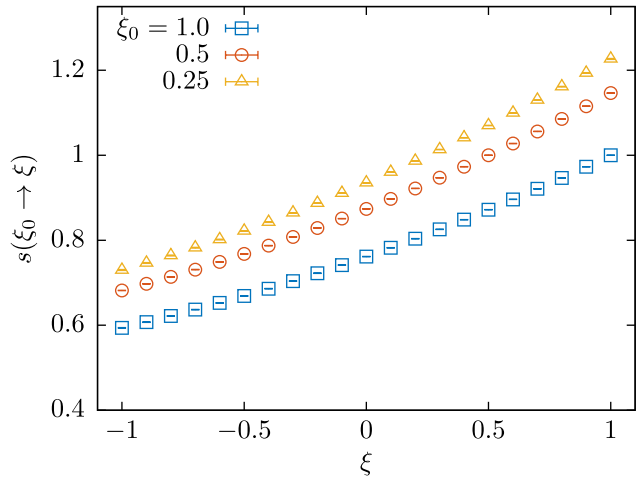

FIG. 4. The generalized sign for simulations at $\xi_0 = 0.25$, 0.5, 1.0 at half-filling on a 2×2 lattice with $U = 10$ and $\beta = 1$.

This formalism then enables direct computation of thermodynamic observables for systems of fictitious particles with different ξ values.

Figure 3 compares the energy density, double occupancy, and AFM structure factor obtained from PIMC simulations with ED results. The benchmark calculations are performed in the canonical ensemble on a 2×2 lattice with PBCs. The particle numbers are fixed to $N_\uparrow = 2$ and $N_\downarrow = 2$ (half-filling) at $U = 10$ and $\beta = 1$. The PIMC simulations are conducted at $\xi_0 = 0.25$, 0.5, and 1.0, while measurements at other ξ are obtained by the reweighting method. The results for all ξ_0 values exhibit excellent agreement with the ED results across the entire range of ξ. As ξ decreases from 1 (bosons) to -1 (fermions), the energy density increases monotonically, while the double occupancy decreases monotonically. This behavior is consistent with the interpretation that quantum exchange statistics effectively induce repulsion, reducing the likelihood of multiple particles occupying the same site. Moreover, the $S(\pi, \pi)$ increases towards the fermionic limit, indicating an enhancement of short-range antiferromagnetic correlations as the system becomes more fermion-like.

Figure 4 shows the generalized sign as a function of ξ for different ξ_0. In the fermion limit $\xi = -1$, the average sign for simulation at $\xi_0 = 0.25$ is larger than that of the other ξ_0 values, i.e., the magnitude of the sign problem is smaller at $\xi_0 = 0.25$. This can be understood by noting that the factor ξ^{N_P} in Eq. (6) strongly suppresses the formation of permutation cycles as ξ decreases [28], thereby reducing the cancellations between positive and negative weights. However, direct simulations near $\xi = 0$ may suffer from low acceptance rates and poor sampling efficiency, despite the improved behavior of the reweighting factor. This trade-off should be considered when choosing the optimal reference ξ_0 for reweighting.

B. Half-filling system

To evaluate the performance of the fictitious-particle PIMC approach, we first study the fictitious-particle Hubbard model at half-filling on larger lattices and across a broad range of parameters. In this regime, the interplay between quantum statistics and strong correlations gives rise to rich physical behavior.

Figure 5 shows the energy density, double occupancy, and structure factor $S(\pi, \pi)$ as functions of the interaction strength U for a 4×4 lattice at inverse temperature $\beta = 1$. Results are presented for three representative limits of quantum statistics: fermions ($\xi = -1$), bosons ($\xi = 1$), and distinguishable particles ($\xi = 0$). These data were obtained by averaging the reweighting results based on multiple simulations at different $\xi_0 > 0$. As will be explained later, the sign problem of the reweighting method is manageable within this parameter regime, and the reweighting method provides reliable estimates of observables across the full range of $\xi \in [-1, 1]$.

For all three particle types, the double occupancy decreases rapidly when $U \gtrsim 10$, indicating the onset of a crossover from a weakly correlated metallic or superfluid regime to a Mott insulating state, where charge fluctuations are strongly suppressed due to the energetic cost of double occupancy. Notably, at fixed U, bosons exhibit the largest double occupancy, followed by distinguishable particles and then fermions, but the energy density of a bosonic system is lower than that in all

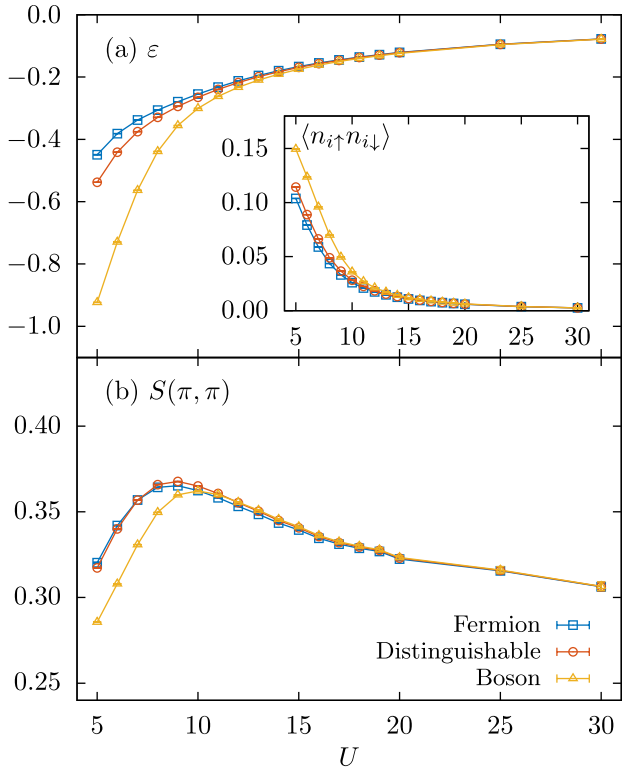

FIG. 5. Various observables as functions of interaction strength U for fermions, bosons, and distinguishable particles on a 4×4 lattice with $\beta = 1$, obtained using the fictitious-particle PIMC. (a) shows the energy density ε, with the inset displaying the double occupancy $\langle n_{i\uparrow} n_{i\downarrow} \rangle$. (b) shows the AFM structure factor $S(\pi, \pi)$. The comparison reveals distinct behaviors among the three statistics, highlighting the role of quantum statistics in correlated many-body systems.

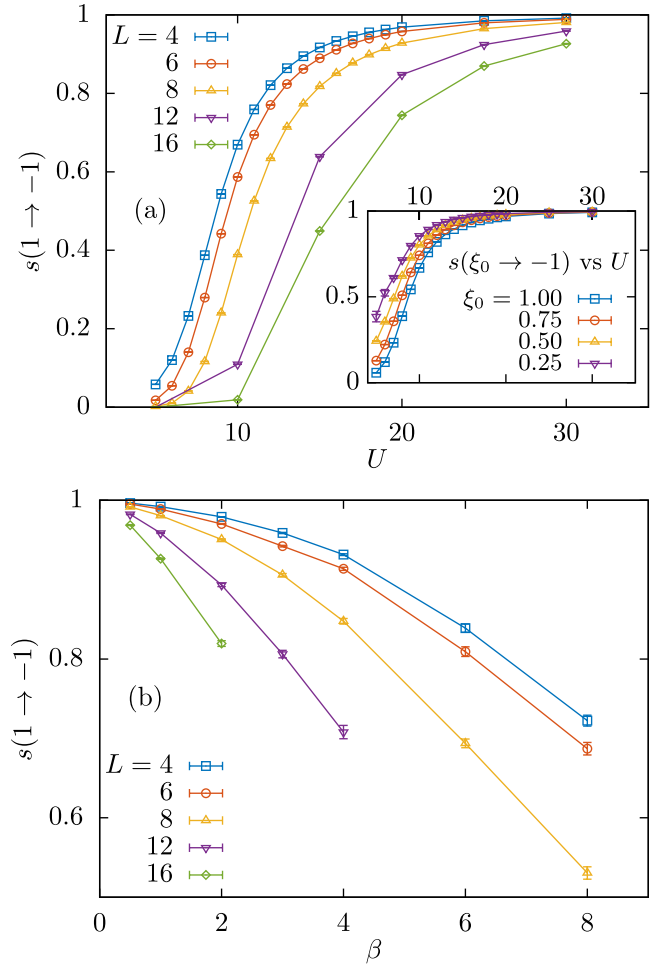

FIG. 6. Average fermion sign of a half-filled system. (a) shows the average sign as a function of U at $\beta = 1$ for various system sizes L, simulated at $\xi_0 = 1$. The sign problem is severe at small U and becomes less pronounced as U increases. The inset shows the average sign for $L = 4$ and $\beta = 1$ obtained from simulations with different ξ_0 values, indicating that simulations with smaller ξ_0 can yield a larger average sign. (b) shows the average sign as a function of β at $U = 30$ for various L, simulated directly at $\xi_0 = 1.0$. The sign problem of direct simulation gets more severe as L and β increase.

other cases. These behaviors indicate that the wave function of particles becomes more localized, as $\xi \to -1$.

The structure factor $S(\pi, \pi)$ exhibits a broad peak around $U \approx 8$ for fermions and distinguishable particles, while for bosons the peak is located at $U \approx 10$. This enhancement indicates the development of short-range AFM correlation associated with the incipient Mott transition, even though true long-range AFM order is absent at the finite temperature and small system size considered here. For $U < 10$, fermions and distinguishable particles exhibit similar values of $S(\pi, \pi)$ while bosons have a much smaller $S(\pi, \pi)$. This suggests that the AFM correlation from configurations with $N_P > 0$ is weaker than those of $N_P = 0$, and their contribution to total $S(\pi, \pi)$ is largely canceled in the fermion limit. In contrast, at larger U, all observables become nearly independent of ξ, indicating that the effects of quantum statistics are strongly suppressed in the strongly interacting limit where charge localization dominates.

Figure 6(a) shows the average sign $s(1 \to -1)$ at half-filling as a function of interaction strength U for various system sizes L at $\beta = 1.0$. As the on-site repulsion U increases, the average sign improves due to the suppression of particle exchanges, which reduces the occurrence of negative weight configurations and thus alleviates the sign problem. In contrast, the sign problem becomes more severe as the system size increases. This can be understood by assuming that particle exchange mostly occurs within a finite length scale; then, the average N_P should increase as $\sim L^2$. As the average N_P increases, the cancellation might become more severe. The inset of Fig. 6 shows the average sign for $L = 4$ and $\beta = 1$ obtained by reweighting from different ξ_0 values. Simulations performed at smaller ξ_0 yield larger average signs.

Figure 6(b) further shows the average sign at $U = 30$ as a function of β for different system sizes with $\xi_0 = 1$. The observed decrease in the average sign with increasing β reflects the fact that quantum exchange effects become more pronounced at lower temperatures, thereby enhancing the sign fluctuation of the configuration weight. Nonetheless, we expect the sign problem to remain manageable down to $\beta \approx 12$ for $L = 4$ and to $\beta \approx 4$ for $L = 16$. In such moderate system

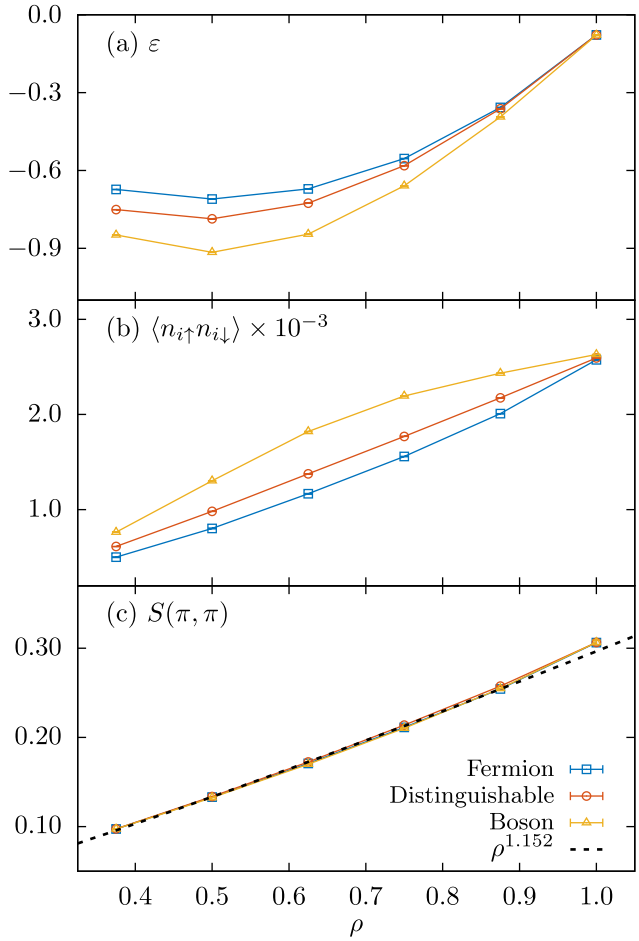

FIG. 7. Various observables as functions of particle density ρ for fermions, bosons, and distinguishable particles on a 4×4 lattice with $\beta = 1$ and $U = 30$: (a) energy density ε, (b) double occupancy $\langle n_{i\uparrow}n_{i\downarrow}\rangle$, and (c) structure factor $S(\pi, \pi)$. The system is unpolarized with equal populations of spin-up and spin-down particles, i.e., $N_\uparrow = N_\downarrow$.

size and temperature, the system could exhibit interesting thermodynamic and dynamical properties [8].

C. Doped system at strong coupling

Based on our findings at half-filling — where ξ reweighting becomes increasingly effective at large U — we further apply the fictitious-particle PIMC method to the hole-doped Hubbard model in the strong-coupling regime, and examine the performance of the reweighting method. Upon doping, the exact mapping to the spin-$\frac{1}{2}$ Heisenberg model at large U no longer holds, and the low-energy physics is instead approximately described by an effective t-J model. This regime can host rich phenomena, such as Nagaoka polarons and kinetic ferromagnetism [8], but also poses serious challenges for existing QMC methods.

Figure 7 illustrates the energy density, the on-site double occupancy, and the AFM staggered structure factor as functions of the total particle density ρ on a 4×4 lattice at $\beta = 1$ and $U = 30$, for fermions ($\xi = -1$), distinguishable particles ($\xi = 0$), and bosons ($\xi = 1$). The particle density is defined as $\rho = (N_\uparrow + N_\downarrow)/L^2$. For simplicity, the system is kept unpolarized with equal populations of the two types of particles, i.e., $N_\uparrow = N_\downarrow$. As shown in Fig. 7(a), over the explored density range, bosons exhibit the lowest energy while fermions have the highest, with distinguishable particles in between. The energy density also shows a minimum at quarter filling $\rho = 0.5$, where the energy difference among the three types of particles is most pronounced. Figure 7(b) shows the double occupancy (scaled by 10^{-3}) as a function of ρ. It can be seen that bosons maintain the highest probability of double occupation, while fermions maintain the lowest. Another intriguing feature is that the curves are concave for bosons, approximately straight for distinguishable particles, and convex for fermions. Figure 7(c) reveals that $S(\pi, \pi)$ almost collapses onto a single curve for all three statistics, closely following a power-law scaling $S(\pi, \pi) \propto \rho^{1.152}$ as shown by the dashed line. This indicates that, in the strong-coupling regime $U \gg t$ of an unpolarized system, short-range correlations are governed predominantly by the particle density and only weakly depend on the quantum exchange statistics.

Figure 8 summarizes how the sign problem evolves with electron density and temperature for unpolarized doped systems at large U. In Fig. 8(a), we show the average sign $s(1 \to -1)$ as a function of particle density ρ for $L = 4, 8, 16, 32$ at $U = 30$ and $\beta = 1$. The curve for $L = 4$ displays a pronounced "U shape": the sign is close to 1 at half-filling, dips to a minimum around $\rho \approx 0.5$, and then recovers as the system is emptied. This can be understood as follows. At half-filling, the sign oscillation is weak, since the particles are mostly localized due to the strong on-site repulsion U and particle permutation is rare. In the dilute limit $\rho \to 0$, the separation between particles is so large that particle exchange is unlikely to occur, which also leads to a weak sign oscillation. However, at the intermediate filling, particle exchanges become more frequent, causing a stronger sign cancellation. The U-shaped ρ dependence of the sign in the fictitious-particle PIMC differs from that of the DQMC at intermediate U, for which various dips occur between $0.5 < \rho < 1.0$ [15]. Furthermore, for a fixed doping, the sign problem becomes more severe as L increases. By $L = 32$, the sign is approximately zero at $1/16$ hole doping, rendering the reweighting scheme inefficient. In Fig. 8(b), we investigate the average sign behavior for a fixed number of dopants. Specifically, the total number of hole dopants is fixed to $N_h = 2$ (one for each spin species) across temperatures $\beta = 1, 2, 3$, and 4 at various system sizes. As the system size increases, the average sign exhibits a nonmonotonic dependence: it initially increases, then decreases slowly. The initial rise is due to the decrease in the effective doping concentration, which pushes the system towards the half-filled limit, where the sign problem is less severe. The latter decline arises as the volume scaling of the sign problem eventually dominates. Crucially, this decay is substantially slower than in the fixed-concentration case, which enables simulations of larger systems and lower temperatures at a fixed number of dopants — a regime essential for investigating the physics of dilute holes. Figure 8(c) further shows the temperature dependence of the average sign for $L = 8$ at $\rho = 0.9375$ and various U. The sign decreases as β increases. For $U = 30$, it drops below 0.01 at $\beta = 4$, making direct reweighting inefficient at $\beta > 4$. For larger on-site repulsion U, however, the

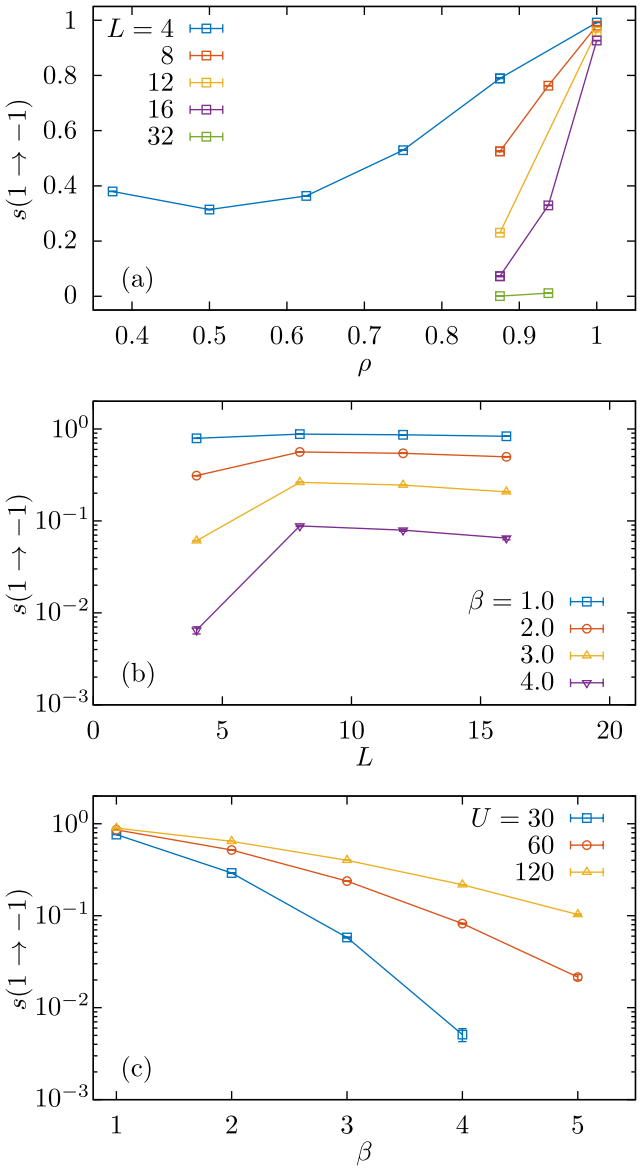

FIG. 8. Average sign for the doped fictitious particle Hubbard model. (a) Average sign versus particle density ρ for various system sizes L at $U = 30$ and $\beta = 1.0$. (b) Average sign versus system size L at $U = 30$ for various β with the total number of hole dopants fixed to $N_h = 2$ (one for each spin species). (c) Average sign versus β at fixed density $\rho = 0.9375$ and $L = 8$ for various interaction strengths U (semilog scale).

sign exhibits a slower decay. For instance, at $U = 120$, the sign remains approximately 0.1 down to $\beta = 5$.

Our analysis demonstrates that the fictitious-particle PIMC method, combined with the ξ-reweighting technique, provides an effective approach for probing the Fermi-Hubbard model, particularly in the large-U regime. In this regime, strong particle localization suppresses spatial exchange processes, which significantly mitigates the severity of the sign problem and facilitates access to fermionic observables via direct reweighting. This behavior renders the method highly suitable for investigating the regime of small doping ($\delta \to 0$) and strong correlation ($U \gg t$), often referred to as the Nagaoka limit. Recent studies have highlighted this regime as a host for emergent phenomena, such as Nagaoka polarons and short-range ferromagnetic correlations at finite temperatures [42]. These observations underscore the potential of the fictitious-particle PIMC framework as a robust tool for exploring emergent physics in the doped, strongly interacting Hubbard model, a regime that remains challenging for many conventional approaches [16,43].

V. EXTRAPOLATION TO FERMION LIMIT

In this section, we assess the performance of the ξ-extrapolation method for the 2D Hubbard model. For various interacting continuum systems, a simple parabolic ansatz for observables,

$$O(T, \xi) = c_0 + c_1\xi + c_2\xi^2, \tag{22}$$

has been shown to be effective for the energy density [25,26] and for other quantities such as correlation functions [28]. However, its applicability and the appropriate polynomial order are not guaranteed for lattice models, especially under strong correlations. To examine this, we test the approach at strong coupling ($U = 30$) and intermediate temperature ($\beta = 1.0$) at 1/8 hole doping. Moreover, unlike the original ξ-extrapolation method, which only utilized the bosonic sector data, we employ a more general strategy that also incorporates data from the fermionic regime to obtain a more controlled extrapolation [44].

We first applied the method to the energy density ε. We start by performing a series of fits for the small system of $L = 4$. In this case, the MC data over the entire ξ range can be accurately obtained using the reweighting technique. As shown in Fig. 9(a), we compare the fit quality of various fitting ansatz and fitting ranges. The simple quadratic ansatz (fit 1) in Eq. (22) does not provide a satisfactory fit to the full range of data for $\xi \in [-1, 1]$. Both the fermionic limit and the bosonic limit show considerable discrepancy. We then change the fitting range by discarding data that is far from the $\xi = -1$ limit, and we find that only by dropping all $\xi > 0$ data can the curve be well fitted using Eq.(22), with $\chi^2/\text{d.o.f.} \approx 1.3$ (fit 2). As suggested in Ref. [26], we also gradually increase the order of the ansatz. We find that a third-order polynomial indeed yields a substantially improved fit over the entire ξ range (fit 3), and a quartic polynomial also provides an excellent fit (fit 4). The ratios between the MC data and the fit curves for fits 3 and 4 are shown in the inset. The quartic fit, however, does not provide a significant qualitative improvement over the cubic fit, suggesting that a third-order polynomial suffices in this case as the extrapolation ansatz. We then fit the $L = 8$ and $L = 16$ data using the cubic polynomial, observing similarly high-quality fits, as shown in Fig. 9(b). This result indicates that, under the given conditions, a cubic polynomial is required to accurately describe the functional dependence of $\varepsilon(\xi)$ in the Hubbard model.

Next, we examine the AFM structure factor $S(\pi, \pi)$ as a function of ξ as shown in Fig. 10. It can be seen that distinguishable particles have the highest $S(\pi, \pi)$, with the fermionic value slightly below the bosonic one. This indicates that even though the quantum exchange effect is suppressed at strong coupling, the presence of holes induces particle

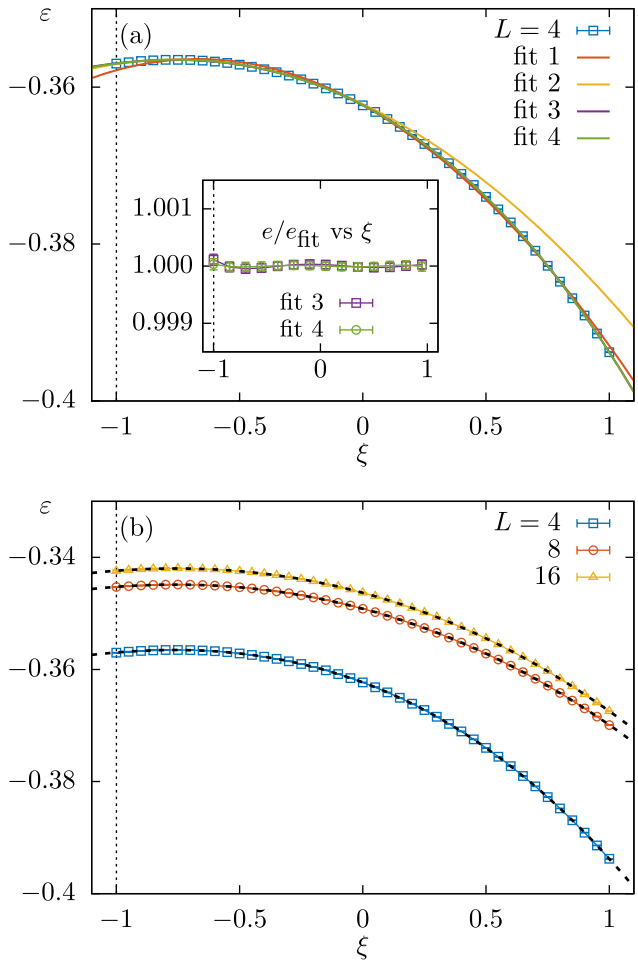

FIG. 9. Energy density ε as functions of ξ at $U = 30$, $\rho = 0.875$, and $\beta = 1.0$. (a) compares different fitting ansatz and fitting ranges. Fit 1 stands for quadratic fit over $\xi \in [-1, 1]$; fit 2 is the quadratic fit over $\xi \in [-1, 0]$; fit 3 is the cubic fit over $\xi \in [-1, 1]$; fit 4 is the quartic fit over $\xi \in [-1, 1]$. The inset shows the ratio between the simulation data and the fitted function for fits 3 and 4. (b) shows the $\varepsilon(\xi)$ curves for various system sizes $L = 4, 8, 16$ can be well-fitted by cubic polynomials over the entire $\xi \in [-1, 1]$ range.

exchanges and reduces the overall AFM correlation. However, this observable is considerably more sensitive to the fermion sign problem. In particular, for $L = 16$ the relative error in $S(\pi, \pi)$ becomes prohibitively large for $\xi < -0.5$, rendering direct reweighting unreliable in this region. To address this limitation, we adopted a systematic extrapolation strategy. For smaller systems with $L = 4, 8$, where the sign problem is less severe, we find that a quadratic polynomial provides an excellent fit for $S(\pi, \pi)$ across the entire ξ range. Based on this observation, we applied the same quadratic ansatz to the $L = 16$ data, restricting the fit to the statistically reliable window $\xi \in [-0.5, 1.0]$ as shown in Fig. 10. Extrapolating this fit to $\xi = -1$, we estimate that $S(\pi, \pi)|_{\xi=-1} \approx 0.2404$ in the fermion limit. Currently, no reliable benchmark data exist in this parameter regime for direct comparison, highlighting the importance of such extrapolations for exploring strongly interacting, doped fermion systems.

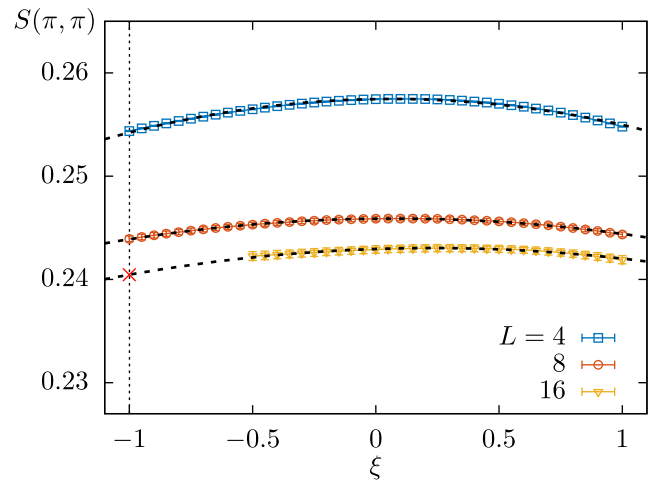

FIG. 10. The AFM structure factor $S(\pi, \pi)$ as functions of ξ at $U = 30$, $\rho = 0.875$, and $\beta = 1.0$ for system sizes $L = 4, 8, 16$. For $S(\pi, \pi)$, the data for $L = 4$ and $L = 8$ can be fitted by a quadratic polynomial over the entire range of ξ. Measurements of $S(\pi, \pi)$ at $\xi < -0.5$ show large statistical uncertainties and are thus not shown. By fitting the statistically reliable regime with a quadratic polynomial, we extrapolate the $S(\pi, \pi)$ to the $\xi = -1$ limit, marked by the red cross.

Our analysis demonstrates that ξ-extrapolation, when combined with reweighting, provides a viable approach for probing the Fermi-Hubbard model. By incorporating data from both the sign-problem-free regime ($\xi \geqslant 0$) and the fermionic sector ($\xi < 0$) obtained via reweighting, we achieve a more controlled and reliable extrapolation. The reliability of the extrapolation also depends on the observable considered and the choice of fitting ansatz. At the considered temperature, we find that a low-order polynomial (quadratic or cubic) suffices to accurately capture the ξ dependence of observables such as the energy density and spin correlations. This suggests that, in this regime, the observable curves remain sufficiently smooth to enable direct extrapolation. However, at lower temperatures, the analytic properties of the fictitious-particle partition function play a more prominent role in limiting the applicability of extrapolation schemes. The partition function $\mathcal{Z}_\xi(T)$ can be reformulated as an $N - 1$ degree polynomial of ξ, which possesses roots (Lee-Yang zeros [45,46]) in the complex ξ plane. These roots move towards the negative real axis as $T \to 0$. In the zero-temperature limit, they produce nonanalytical behaviors exactly at $\xi = -1, -1/2, \ldots, -1/(N-1)$ for a system with N identical particles, corresponding to the sudden vanishing of the weight of the symmetric ground state at these points. See the Appendix for details. The presence of these singularities near the real axis thereby hinders direct polynomial extrapolation from the bosonic sector to the fermionic limit. In such regimes, more advanced strategies may be required [31,32].

VI. DISCUSSION AND CONCLUSION

This work demonstrates that the fictitious-particle PIMC method, a conceptually simple approach, is surprisingly effective for studying the two-dimensional Hubbard model at

strong coupling. As the interaction strength U increases, the fermion sign problem becomes less severe due to suppressed particle exchange, allowing direct ξ-reweighting to remain viable even in doped systems at moderate temperatures. For parameter regimes where the sign problem is severe, we show that combining reweighting with ξ extrapolation enables a more controlled and reliable extrapolation to the fermion limit. Specifically, we find that ξ extrapolation with a low-order polynomial ansatz suffices for accurate results. For instance, at $U = 30$, $\beta = 1$, and $\rho = 0.875$, a third-order ansatz accurately describes the energy across the full range of ξ, while a quadratic fit captures the AFM structure factor. These results establish the validity of the ξ-extrapolation method for lattice fermions and extend the applicability of the fictitious-particle framework.

It is instructive to place the fictitious-particle PIMC within the context of existing numerical techniques. While DQMC algorithms remain highly efficient for half-filled Fermi-Hubbard systems, our approach offers unique features that complement auxiliary-field methods. Notably, the introduction of the continuous parameter ξ facilitates a systematic exploration of exchange statistics and enhances data analysis in the fermionic limit through ξ extrapolation, whose application on lattice models remains to be further explored. Additionally, the PIMC framework naturally accommodates the canonical ensemble, enabling the study of many-body effects at fixed particle numbers, a favorable feature for benchmarking against cold-atom experiments. Finally, working directly in the path-integral representation also allows the algorithm to avoid the matrix ill-conditioning common in strongly interacting regimes, while maintaining a time complexity of $\mathcal{O}(L^d\beta)$. These distinctive features make the fictitious-particle PIMC a valuable complement to existing methods, especially for exploring parameter regimes that are challenging for conventional algorithms, such as the Nagaoka ferromagnet in the infinite-U limit [8,47–49].

We also note that several difficulties remain in studying the lattice model using the fictitious-particle PIMC method. At large U, though the sign problem is small due to suppressed particle exchange, the acceptance ratio of certain worm updates can be reduced. The worldline configuration for virtual exchange of spins can be difficult to sample using the standard worm-update scheme. A small segment with double occupancy is severely penalized by an exponential factor of U. To overcome these sampling bottlenecks, advanced techniques such as directed-loop algorithms or cluster-style moves are promising next steps [50]. On the other hand, at lower temperatures, both reweighting and ξ extrapolation become increasingly delicate, suggesting that further tempered extrapolation strategies will be necessary to access this regime. Searching for strategies to expand the accessible parameter regime and validating them constitutes the current frontier of fictitious-particle-based Monte Carlo methods. Further possible improvements may involve incorporating additional tools for fermion PIMC simulations to mitigate cancellations due to particle exchange, such as the permutation-blocking paradigm [51].

The underlying formalism of the fictitious-particle PIMC is also highly versatile. While simulations in the canonical ensemble with appropriate finite-size corrections are sufficient to describe experimentally relevant systems, extending the formulation to the grand-canonical ensemble offers additional practical benefits. It allows direct comparison with conventional DQMC methods and helps optimize the update efficiency of canonical simulations. Moreover, performing N_P-resolved measurements could provide insight into how different permutation sectors contribute to the overall sign cancellations, thereby offering a deeper understanding of the sign problem in relevant systems. In addition, the fictitious-particle PIMC provides a natural method for studying the effect of particle distinguishability [52,53], which is separated from other quantum effects in the path-integral formulation, as a function of the parameter ξ. This can provide novel insights for the emergence of exotic quantum phases in quantum many-body systems.

Note added. Recently, we note that a reweighting-based estimator within the fictitious-particle PIMC framework was independently introduced by Dornheim *et al.* [54].

ACKNOWLEDGMENTS

We thank Y. Xiong, H. Xiong, and T. Morresi for useful discussions. We acknowledge the support by the National Natural Science Foundation of China (NSFC) under Grants No. 12204173 and No. 12275263, as well as the Quantum Science and Technology-National Science and Technology Major Project Grant No. 2021ZD0301900. Y.D. is also supported by the Natural Science Foundation of Fujian Province 802 of China (Grant No. 2023J02032). Z.F. is also supported by National Natural Science Foundation of China (NSFC) under Grant No. 12504265.

DATA AVAILABILITY

The data that support the findings of this article are openly available [55].

APPENDIX: LOW-TEMPERATURE PROPERTIES OF FICTITIOUS PARTICLE PARTITION FUNCTION

To provide a theoretical basis for the limitations of the ξ-extrapolation discussed in Sec. V, we analyze the analytic structure of the fictitious-particle partition function $\mathcal{Z}_\xi(T)$. The following discussion is formulated in a model-independent manner to clarify how the intrinsic properties of $\mathcal{Z}_\xi(T)$ dictate the convergence of extrapolation schemes. Here, our analysis assumes that the Hamiltonian is fully symmetric under the permutation group S_N [56], so that all permutation sectors ($N_P = 0, 1, \ldots, N-1$) can, in principle, contribute to the sum.

We start by reformulating the partition function to resolve contributions from different eigenstates:

$$\mathcal{Z}_\xi(T) = \frac{1}{N!}\sum_{P\in S_N}\sum_i \xi^{N_P}\langle\Psi_i|e^{-\beta\mathcal{H}}|P(\Psi_i)\rangle \tag{A1}$$

$$= \frac{1}{N!}\sum_{P\in S_N}\sum_i \xi^{N_P}\sum_j \langle\Psi_i|j\rangle e^{-\beta\varepsilon_j}\langle j|P(\Psi_i)\rangle \tag{A2}$$

$$= \frac{1}{N!}\sum_j e^{-\beta\varepsilon_j}\sum_{P\in S_N}\xi^{N_P}\sum_i \langle j|P(\Psi_i)\rangle\langle\Psi_i|j\rangle, \tag{A3}$$

where $|j\rangle$ is the eigenstate of $\mathcal{H}$ with energy ε_j. We define the self-overlap factor $a(j,P) \equiv \sum_i \langle j|P(\Psi_i)\rangle\langle\Psi_i|j\rangle$, which measures the projection of $|j\rangle$ onto its permuted representation in the chosen basis. The sum $\sum_i |P(\Psi_i)\rangle\langle\Psi_i|$ is the projection matrix of permutation P, which projects a wave function from the original basis to a permuted basis. The partition function can then be expressed as

$$\mathcal{Z}_\xi(T) = \frac{1}{N!}\sum_j e^{-\beta\varepsilon_j}\sum_{P\in S_N}\xi^{N_P}a(j,P) \tag{A4}$$

$$= \sum_j e^{-\beta\varepsilon_j}\lambda_j(\xi), \tag{A5}$$

where

$$\lambda_j(\xi) = \frac{1}{N!}\sum_{P\in S_N}\xi^{N_P}a(j,P) \tag{A6}$$

is a polynomial of degree $N-1$ in ξ that encodes the symmetry of $|j\rangle$ under S_N. It controls the weight of the eigenstate in the partition function. For example, a fully bosonic eigenstate satisfies $\lambda_j(1)=1$ and $\lambda_j(-1)=0$, so its contribution vanishes in the fermionic limit.

By grouping permutations by the cycle number N_P, the generalized partition function can be written as an $(N-1)$-th degree polynomial in ξ:

$$\mathcal{Z}_\xi(T) = \sum_{s=0}^{N-1} c(s,\beta)\xi^s, \tag{A7}$$

where $c(s,\beta)$ collects contributions from all permutations with $N_P = s$. The roots of this polynomial correspond to Lee-Yang zeros [45,46]. If the nearest zeros lie close to the real axis, they induce nonanalytic behavior in observables $O(\xi)$, thereby destabilizing direct ξ extrapolation.

In the limit $T\to 0$, the ξ dependence of the partition function is dominated by the ground state. We analyze the partition function of the one-dimensional (1D) and 2D noninteracting lattice fermions with or without a hardcore constraint using exact diagonalization. The numerical analysis reveals that the partition function at low temperatures seems to have roots on the negative real axis at $-1, -\frac{1}{2}, -\frac{1}{3}, \cdots, -\frac{1}{N-1}$. This phenomenon can be understood as follows. For a fully permutation-symmetric Hamiltonian, the unrestricted ground state is bosonic [56], implying $a(0,P)=1$ for all P. The coefficients of $\lambda_0(\xi)$ polynomial are then given by the number of cyclic decompositions of the permutation group, which is related to the first Stirling number $s(N, N-N_P)$. The minimum number of pairwise swaps equals $N-N_c$, where N_c is the number of cycles in the permutation. The generator of unsigned Stirling numbers of the first kind is

$$x(x+1)(x+2)...(x+N-1) = \sum_{N_c=0}^{N-1}|s(N,N_c)|x^{N_c}. \tag{A8}$$

We then have $|s(N,N-N_P)|$ permutations with a given N_P. In the $T\to 0$ limit, the partition function can be written as

$$\mathcal{Z}_\xi(T) \approx \frac{1}{N!}e^{-\beta\varepsilon_0}\sum_{N_P=0}^{N-1}|s(N,N-N_P)|\xi^{N_P} \tag{A9}$$

$$= \frac{1}{N!}e^{-\beta\varepsilon_0}\xi^N\sum_{N_P=0}^{N-1}|s(N,N-N_P)|\xi^{N_P-N} \tag{A10}$$

$$= \frac{1}{N!}e^{-\beta\varepsilon_0}(1+\xi)(1+2\xi)...(1+(N-1)\xi) \tag{A11}$$

$$= \frac{1}{N}e^{-\beta\varepsilon_0}(\xi+1)\left(\xi+\frac{1}{2}\right)...\left(\xi+\frac{1}{N-1}\right). \tag{A12}$$

Thus, the contribution of spatially symmetric ground state vanishes at $\xi = -1, -1/2, \ldots, -1/(N-1)$. This implies that at these specific points, the partition function is no longer determined by the spatially symmetric ground state, but rather by higher-energy eigenstates with nonvanishing contributions. This transition signals a change in the dominant eigenstate, leading to nonanalytic behavior of $\mathcal{Z}_\xi$ and effectively invalidating simple polynomial extrapolation schemes based on bosonic-sector simulations. At finite temperatures, excited states shift these zeros into the complex plane. Direct ξ extrapolation remains feasible as long as the nearest zeros are sufficiently far from the real axis relative to statistical noise. Finally, we note that a concurrent work [57] recently provided a mathematical proof for this zero distribution using a recursion relation approach. Our derivation above provides independent verification based on the combinatorial properties of the symmetric group, confirming the robustness of this result.

[1] W. M. C. Foulkes, L. Mitas, R. J. Needs, and G. Rajagopal, Quantum Monte Carlo simulations of solids, Rev. Mod. Phys. **73**, 33 (2001).

[2] A. W. Sandvik, Computational studies of quantum spin systems, AIP Conf. Proc. **1297**, 135 (2010).

[3] J. Carlson, S. Gandolfi, F. Pederiva, S. C. Pieper, R. Schiavilla, K. E. Schmidt, and R. B. Wiringa, Quantum Monte Carlo methods for nuclear physics, Rev. Mod. Phys. **87**, 1067 (2015).

[4] E. Y. Loh, J. E. Gubernatis, R. T. Scalettar, S. R. White, D. J. Scalapino, and R. L. Sugar, Sign problem in the numerical simulation of many-electron systems, Phys. Rev. B **41**, 9301 (1990).

[5] M. Troyer and U.-J. Wiese, Computational complexity and fundamental limitations to fermionic quantum Monte Carlo simulations, Phys. Rev. Lett. **94**, 170201 (2005).

[6] J. Hubbard, Electron correlations in narrow energy bands, Proc. R. Soc. London Ser. A **276**, 238 (1963).

[7] B. Keimer, S. A. Kivelson, M. R. Norman, S. Uchida, and J. Zaanen, From quantum matter to high-temperature superconductivity in copper oxides, Nature (London) **518**, 179 (2015).

[8] D. P. Arovas, E. Berg, S. A. Kivelson, and S. Raghu, The Hubbard model, Annu. Rev. Condens. Matter Phys. **13**, 239 (2022).

[9] J. P. F. LeBlanc, A. E. Antipov, F. Becca, I. W. Bulik, G. K.-L. Chan, C.-M. Chung, Y. Deng, M. Ferrero, T. M. Henderson,

C. A. Jiménez-Hoyos, E. Kozik, X.-W. Liu, A. J. Millis, N. V. Prokof'ev, M. Qin, G. E. Scuseria, H. Shi, B. V. Svistunov, L. F. Tocchio, I. S. Tupitsyn, *et al.*, Solutions of the two-dimensional Hubbard model: Benchmarks and results from a wide range of numerical algorithms, Phys. Rev. X **5**, 041041 (2015).

[10] M. Qin, T. Schäfer, S. Andergassen, P. Corboz, and E. Gull, The Hubbard model: A computational perspective, Annu. Rev. Condens. Matter Phys. **13**, 275 (2022).

[11] A. Bohrdt, L. Homeier, C. Reinmoser, E. Demler, and F. Grusdt, Exploration of doped quantum magnets with ultracold atoms, Ann. Phys. (NY) **435**, 168651 (2021).

[12] H.-J. Shao, Y.-X. Wang, D.-Z. Zhu, Y.-S. Zhu, H.-N. Sun, S.-Y. Chen, C. Zhang, Z.-J. Fan, Y. Deng, X.-C. Yao, Y.-A. Chen, and J.-W. Pan, Antiferromagnetic phase transition in a 3D fermionic Hubbard model, Nature (London) **632**, 267 (2024).

[13] R. Blankenbecler, D. J. Scalapino, and R. L. Sugar, Monte Carlo calculations of coupled boson-fermion systems. I, Phys. Rev. D **24**, 2278 (1981).

[14] J. E. Hirsch, Discrete Hubbard-Stratonovich transformation for fermion lattice models, Phys. Rev. B **28**, 4059 (1983).

[15] S. R. White, D. J. Scalapino, R. L. Sugar, E. Y. Loh, J. E. Gubernatis, and R. T. Scalettar, Numerical study of the two-dimensional Hubbard model, Phys. Rev. B **40**, 506 (1989).

[16] F. Assaad and H. Evertz, World-line and determinantal quantum Monte Carlo methods for spins, phonons and electrons, in *Computational Many-Particle Physics*, edited by H. Fehske, R. Schneider, and A. Weiße (Springer, Berlin, 2008), Vol. 739, pp. 277–356.

[17] Z.-X. Li and H. Yao, Sign-problem-free fermionic quantum Monte Carlo: Developments and applications, Annu. Rev. Condens. Matter Phys. **10**, 337 (2019).

[18] G. Pan and Z. Y. Meng, The sign problem in quantum Monte Carlo simulations, in *Encyclopedia of Condensed Matter Physics*, 2nd ed. edited by T. Chakraborty (Academic, Oxford, 2024), pp. 879–893.

[19] E. Kozik, K. Van Houcke, E. Gull, L. Pollet, N. Prokof'ev, B. Svistunov, and M. Troyer, Diagrammatic Monte Carlo for correlated fermions, Europhys. Lett. **90**, 10004 (2010).

[20] M. V. Ulybyshev and S. N. Valgushev, Path integral representation for the Hubbard model with reduced number of Lefschetz thimbles, arXiv:1712.02188.

[21] M. Ulybyshev, C. Winterowd, and S. Zafeiropoulos, Lefschetz thimbles decomposition for the Hubbard model on the hexagonal lattice, Phys. Rev. D **101**, 014508 (2020).

[22] Z.-X. Li, Y.-F. Jiang, and H. Yao, Solving the fermion sign problem in quantum Monte Carlo simulations by Majorana representation, Phys. Rev. B **91**, 241117(R) (2015).

[23] Y.-Y. He, M. Qin, H. Shi, Z.-Y. Lu, and S. Zhang, Finite-temperature auxiliary-field quantum Monte Carlo: Self-consistent constraint and systematic approach to low temperatures, Phys. Rev. B **99**, 045108 (2019).

[24] X. Zhang, G. Pan, X. Y. Xu, and Z. Y. Meng, Fermion sign bounds theory in quantum Monte Carlo simulation, Phys. Rev. B **106**, 035121 (2022).

[25] Y. Xiong and H. Xiong, On the thermodynamic properties of fictitious identical particles and the application to fermion sign problem, J. Chem. Phys. **157**, 094112 (2022).

[26] Y. Xiong and H. Xiong, Parametrized path integral formulation for large fermion systems, arXiv:2208.13777.

[27] Y. Xiong, S. Liu, and H. Xiong, Quadratic scaling path integral molecular dynamics for fictitious identical particles and its application to fermion systems, Phys. Rev. E **110**, 065303 (2024).

[28] T. Dornheim, P. Tolias, S. Groth, Z. A. Moldabekov, J. Vorberger, and B. Hirshberg, Fermionic physics from *ab initio* path integral Monte Carlo simulations of fictitious identical particles, J. Chem. Phys. **159**, 164113 (2023).

[29] T. Dornheim, S. Schwalbe, Z. A. Moldabekov, J. Vorberger, and P. Tolias, *Ab Initio* path integral Monte Carlo simulations of the uniform electron gas on large length scales, J. Phys. Chem. Lett. **15**, 1305 (2024).

[30] T. Dornheim, T. Döppner, P. Tolias, M. P. Böhme, L. B. Fletcher, T. Gawne, F. R. Graziani, D. Kraus, M. J. MacDonald, Z. A. Moldabekov, S. Schwalbe, D. O. Gericke, and J. Vorberger, Unraveling electronic correlations in warm dense quantum plasmas, Nat. Commun. **16**, 5103 (2025).

[31] Y. Xiong and H. Xiong, Thermodynamics of fermions at any temperature based on parametrized partition function, Phys. Rev. E **107**, 055308 (2023).

[32] T. Morresi and G. Garberoglio, Normal liquid ^{3}He studied by path-integral Monte Carlo with a parametrized partition function, Phys. Rev. B **111**, 014521 (2025).

[33] T. Ying, The sign problem in quantum Monte Carlo simulations of the Hubbard model in a weak interaction region, Europhys. Lett. **125**, 27001 (2019).

[34] D. M. Ceperley and E. L. Pollock, Path-integral simulation of the superfluid transition in two-dimensional ^{4}He, Phys. Rev. B **39**, 2084 (1989).

[35] N. Prokof'ev, B. Svistunov, and I. Tupitsyn, "Worm" algorithm in quantum Monte Carlo simulations, Phys. Lett. A **238**, 253 (1998).

[36] M. Boninsegni, N. Prokof'ev, and B. Svistunov, Worm algorithm for continuous-space path integral Monte Carlo simulations, Phys. Rev. Lett. **96**, 070601 (2006).

[37] N. Prokof'ev and B. Svistunov, Worm algorithms for classical statistical models, Phys. Rev. Lett. **87**, 160601 (2001).

[38] B. Capogrosso-Sansone, Ş. G. Söyler, N. Prokof'ev, and B. Svistunov, Monte carlo study of the two-dimensional Bose-Hubbard model, Phys. Rev. A **77**, 015602 (2008).

[39] P. E. Kornilovitch, Path-integral approach to lattice polarons, J. Phys.: Condens. Matter **19**, 255213 (2007).

[40] Y. Yanay, E. J. Mueller, and V. Elser, Magnetic polarons in two-component hard-core bosons, Phys. Rev. A **87**, 043622 (2013).

[41] T.-S. Zeng, Integer quantum Hall effect of two-component hard-core bosons in a topological triangular lattice, Phys. Rev. B **105**, 235140 (2022).

[42] R. C. Newby and E. Khatami, Finite-temperature kinetic ferromagnetism in the square-lattice Hubbard model, Phys. Rev. B **111**, 245120 (2025).

[43] E. Khatami, R. T. Scalettar, and R. R. P. Singh, Finite-temperature superconducting correlations of the Hubbard model, Phys. Rev. B **91**, 241107(R) (2015).

[44] T. Dornheim, Z. Moldabekov, S. Schwalbe, P. Tolias, and J. Vorberger, Fermionic free energies from *ab initio* path integral Monte Carlo simulations of fictitious identical particles, J. Chem. Theory Comput. **21**, 7290 (2025).

[45] C. N. Yang and T. D. Lee, Statistical theory of equations of state and phase transitions. I. Theory of condensation, Phys. Rev. **87**, 404 (1952).

[46] T. D. Lee and C. N. Yang, Statistical theory of equations of state and phase transitions. II. Lattice gas and ising model, Phys. Rev. **87**, 410 (1952).

[47] Y. Nagaoka, Ferromagnetism in a narrow, almost half-filled *s* band, Phys. Rev. **147**, 392 (1966).

[48] D. J. Thouless, Exchange in solid 3He and the Heisenberg Hamiltonian, Proc. Phys. Soc. **86**, 893 (1965).

[49] H. Tasaki, Extension of Nagaoka's theorem on the large- U Hubbard model, Phys. Rev. B **40**, 9192 (1989).

[50] N. Sadoune and L. Pollet, Efficient and scalable path integral Monte Carlo simulations with worm-type updates for bose-Hubbard and XXZ models, SciPost Phys. Codebases 9 (2022).

[51] T. Dornheim, S. Groth, A. Filinov, and M. Bonitz, Permutation blocking path integral Monte Carlo: A highly efficient approach to the simulation of strongly degenerate non-ideal fermions, New J. Phys. **17**, 073017 (2015).

[52] M. Boninsegni, L. Pollet, N. Prokof'ev, and B. Svistunov, Role of Bose statistics in crystallization and quantum jamming, Phys. Rev. Lett. **109**, 025302 (2012).

[53] A. J. Menssen, A. E. Jones, B. J. Metcalf, M. C. Tichy, S. Barz, W. S. Kolthammer, and I. A. Walmsley, Distinguishability and many-particle interference, Phys. Rev. Lett. **118**, 153603 (2017).

[54] T. Dornheim, P. Svensson, P. Hamann, S. Schwalbe, Z. A. Moldabekov, P. Tolias, and J. Vorberger, Reweighting estimator for *ab initio* path integral Monte Carlo simulations of fictitious identical particles, J. Chem. Phys. **163**, 154101 (2025).

[55] Z. Fan, T. Xiao, and Y. Deng, Data of the article titled "Quantum path-integral method for the fictitious-particle Hubbard model" [Data set], Zenodo (2026), https://doi.org/10.5281/zenodo.18695174.

[56] E. H. Lieb and R. Seiringer, *The Stability of Matter in Quantum Mechanics*, 1st ed. (Cambridge University Press, Cambridge, 2009).

[57] R.-C. He, J.-X. Zeng, S. Yang, C. Wang, Q.-J. Ye, and X.-Z. Li, Fermion sign problem and the structure of Lee-Yang zeros: The form of the partition function for indistinguishable particles and its zeros at 0 K, Phys. Rev. E **113**, 024115 (2026.